Monomeric G protein-coupled receptor rhodopsin in solution activates its G protein transducin at the diffusion limit

Oliver P. Ernst[†‡], Verena Gramse[†], Michael Kolbe[§], Klaus Peter Hofmann[†], and Martin Heck[†]

[†]Institut für Medizinische Physik und Biophysik, Charité–Universitätsmedizin Berlin, Charitéplatz 1, D-10117 Berlin, Germany; and
[§]Department of Cellular Microbiology, Max-Planck-Institut für Infektionsbiologie, Charitéplatz 1, D-10117 Berlin, Germany

Edited by Robert J. Lefkowitz, Duke University Medical Center, Durham, NC, and approved May 8, 2007 (received for review March 5, 2007)

G protein-coupled receptors mediate biological signals by stimulating nucleotide exchange in heterotrimeric G proteins ($G\alpha\beta\gamma$). Receptor dimers have been proposed as the functional unit responsible for catalytic interaction with $G\alpha\beta\gamma$. To investigate whether a G protein-coupled receptor monomer can activate $G\alpha\beta\gamma$, we used the retinal photoreceptor rhodopsin and its cognate G protein transducin (G_t) to determine the stoichiometry of rhodopsin/G_t binding and the rate of catalyzed nucleotide exchange in G_t. Purified rhodopsin was prepared in dodecyl maltoside detergent solution. Rhodopsin was monomeric as concluded from fluorescence resonance energy transfer, copurification studies with fluorescent labeled and unlabeled rhodopsin, size exclusion chromatography, and multiangle laser light scattering. A 1:1 complex between light-activated rhodopsin and G_t was found in the elution profiles, and one molecule of GDP was released upon complex formation. Analysis of the speed of catalytic rhodopsin/G_t interaction yielded a maximum of $\approx$50 G_t molecules per second and molecule of activated rhodopsin. The bimolecular rate constant is close to the diffusion limit in the diluted system. The results show that the interaction of G_t with an activated rhodopsin monomer is sufficient for fully functional G_t activation. Although the activation rate in solution is at the physically possible limit, the rate in the native membrane is still 10-fold higher. This is likely attributable to the precise orientation of the G protein to the membrane surface, which enables a fast docking process preceding the actual activation step. Whether docking in membranes involves the formation of rhodopsin dimers or oligomers remains to be elucidated.

enzyme catalysis | nucleotide exchange | light scattering

G protein-coupled receptors (GPCRs) constitute the largest group of transmembrane receptors. These seven-transmembrane helix proteins are involved in detecting a wide variety of chemical and physical stimuli, ranging from ligand binding to light perception (1). In their active state, GPCRs catalyze nucleotide exchange in heterotrimeric G proteins ($G\alpha\beta\gamma$) and thereby route extracellular signals to distinct intracellular signaling pathways (2). Rhodopsin is the prototype and eponym of the largest class of GPCRs, the rhodopsin-like GPCRs (class A). Together with its cognate G protein transducin (G_t), it is part of the visual signaling system found on the disk membranes in the outer segment of vertebrate rod photoreceptor cells. Rhodopsin is activated by photon absorption, causing cis-trans isomerization of the chromophore 11-*cis*-retinal, which is bound covalently to the apoprotein opsin. Optimal photon absorption of photoreceptor cells is ensured by the high density of rhodopsin in the disk membranes [>25,000 receptors per μm^2 (3)].

In disk membranes on mica support, rows of rhodopsin dimers were observed by atomic force microscopy (4). Different types of dimers also were found in crystal structures of rhodopsin (see ref. 5 and references therein). Such direct structural analysis of a GPCR currently is available only for rhodopsin. However, other GPCRs also were found to associate as dimers and higher-order oligomers in living cells (see, e.g., refs. 6–8), although monomers prevail at low expression levels (9, 10). Molecular modeling (11–13), FRET measurements (14–16), and biochemical approaches (5, 17, 18) are consistent with a model in which dimers or higher-order oligomers of rhodopsin, or class A GPCRs in general, constitute the functional unit for G protein activation (19–21). Although this paradigm has been questioned (10, 22, 23), a supramolecular organization of GPCRs indeed may enhance the performance and fidelity with which signals are transferred to the G protein in signal transduction modules (11, 24). Using a simplified system, namely monomeric rhodopsin in detergent solution, we have tested whether such organization of rhodopsin is necessary for efficient catalytic activation of G_t, i.e., nucleotide exchange in the α-subunit of G_t by interaction with light-activated rhodopsin (R*).

Results

Preparation of Monomeric Rhodopsin in Detergent Solution. Rhodopsin used in this study was either prepared from bovine disk membranes or expressed as its apoprotein opsin in COS-1 cells and reconstituted with 11-*cis*-retinal. For solubilization and purification of rhodopsin, we used *n*-dodecyl-β-D-maltopyranoside (DDM) detergent and an immunoaffinity procedure, respectively. We found that the obtained rhodopsin was monomeric, as shown by several lines of evidence:

i. No FRET was observed when opsin apoproteins fused to monomeric variants of enhanced cyan fluorescent protein (mECFP) or yellow fluorescent protein (mVenus), respectively, were coexpressed in COS-1 cells, reconstituted with 11-*cis*-retinal, and copurified in DDM solution. In contrast, a positive FRET control consisting of a purified mVenus–mECFP fusion showed FRET (Fig. 1). Also, when expressed in COS-1 cells, fluorescent opsin fusion proteins in the cell membrane showed FRET (15), indicating a quaternary structure in these membranes.

ii. To verify that our purification protocol yielded monomeric rhodopsin, we performed coexpression and copurification with rhodopsin and the rhodopsin–mVenus fusion protein

Author contributions: O.P.E., V.G., and M.K. contributed equally to this work. O.P.E., V.G., K.P.H., and M.H. designed research; O.P.E., V.G., M.K., and M.H. performed research; M.K. contributed new analytical tools; O.P.E., V.G., M.K., K.P.H., and M.H. analyzed data; and O.P.E., K.P.H., and M.H. wrote the paper.

The authors declare no conflict of interest.

This article is a PNAS Direct Submission.

Abbreviations: $G\alpha\beta\gamma$, heterotrimeric G protein; G_t, transducin; GPCR, G protein-coupled receptor; R*, light-activated rhodopsin; DDM, *n*-dodecyl-β-D-maltopyranoside; SEC, size exclusion chromatography; MALLS, multiangle laser light scattering; mECFP, monomeric variants of enhanced cyan fluorescent protein.

‡To whom correspondence should be addressed. E-mail: oliver.ernst@charite.de.

This article contains supporting information online at www.pnas.org/cgi/content/full/0701967104/DC1.

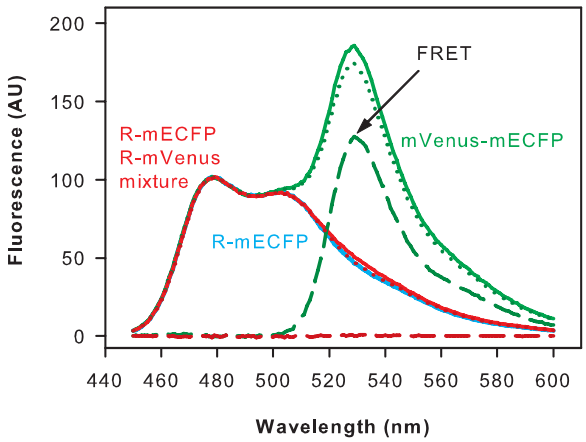

Fig. 1. FRET experiments. Monomeric cyan or yellow variants of GFP fused to the opsin C terminus (R–mECFP and R–mVenus, respectively) were expressed separately and together in COS-1 cells, reconstituted with 11-*cis*-retinal, and purified. Normalized emission spectra (excitation at 420 nm) are shown for purified R–mECFP (cyan line), copurified R–mECFP/R–mVenus (red line), and a fusion protein consisting of mECFP and mVenus as positive FRET control (green line). The spectra of proteins containing an mVenus moiety were corrected for direct excitation of mVenus by the 420 nm excitation beam as described in *Materials and Methods*. FRET is reflected in the difference between the corrected spectra (dotted lines) and the spectrum of R–mECFP (cyan line). These difference spectra (broken lines) show that FRET only occurs in the mVenus–mECFP positive FRET control but not in the R–mECFP/R–mVenus sample. FRET also was lacking in copurified R–mECFP/R–mVenus after illumination of the sample for 15 s with orange light (data not shown).

(Fig. 2). Using unmodified rhodopsin as a purification handle, it was not possible to copurify rhodopsin–mVenus fusion protein lacking a C-terminal affinity tag, which argues again for rhodopsin monomers in solution.

iii. The immunoaffinity purification protocol then was used to purify native rhodopsin from bovine rod cells. Size exclusion chromatography (SEC) of the purified rhodopsin revealed high homogeneity and purity of the preparation as indicated by the absorption spectrum (Fig. 3*A*).

iv. Further analysis by SEC in combination with multiangle laser light scattering (MALLS) detection showed that only monomers were present in the main elution peak of dark state rhodopsin (Fig. 3*B*). MALLS evaluation of each elution slice (Fig. 3*B*) revealed for the central part of the elution peak that protein monomers (experimental mass ≈35 kDa; theoretical mass ≈39 kDa; Fig. 3*B*, red circles) are enclosed by a detergent micelle on the scale of ≈74 kDa (Fig. 3*B*, green circles), yielding a rhodopsin–detergent complex of ≈110 kDa (Fig. 3*B*, black circles). The monomeric nature of rhodopsin remained unaffected after light-activating it directly before the SEC run.

Stoichiometry of Interaction Between Monomeric Rhodopsin and Transducin. We analyzed the interaction of monomeric rhodopsin with G_t by SEC (Fig. 4). SEC first was performed with inactive dark state rhodopsin mixed with inactive GDP-bound G_t (Fig. 4*A*). To study the interaction of R* with G_t, the mixture of rhodopsin and G_t was illuminated with orange light immediately before SEC to produce R*. Interaction between R* and G_t was observed as a shift of the elution peak to a lower elution volume attributable to R*·G_t complex formation (Fig. 4*B*). The different absorption maxima of proteins (280 nm) and retinal chromophore (380 nm; as part of R*) allowed us to determine a stoichiometry of 1:1 for R* and G_t in the main peak containing the protein complex (see Fig. 4 legend and *Materials and Methods* for details). The equimolar R*:G_t stoichiometry was confirmed further by analysis of GDP release upon R*·G_t complex formation (Fig. 4*C*). The amount of R*·G_t complex formed is reflected in the area of the elution peak detected at 380 nm (absorption

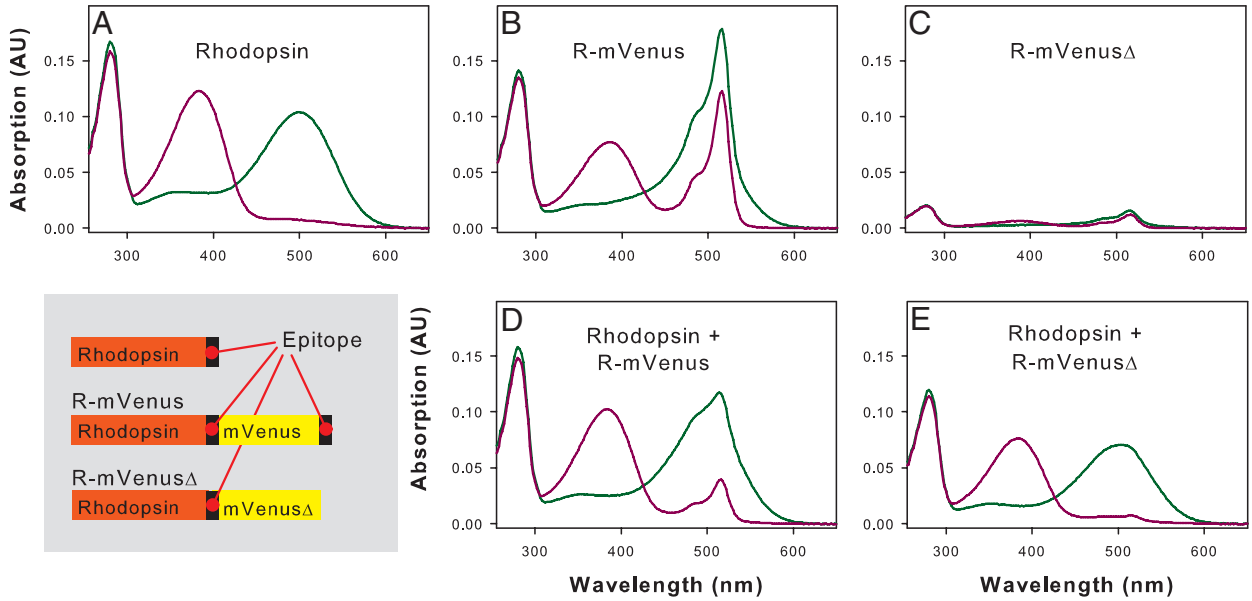

Fig. 2. UV/visible absorption spectra of rhodopsin and different rhodopsin–mVenus fusion proteins after expression in COS-1 cells, reconstitution with 11-*cis*-retinal and purification. The proteins contained one or two epitopes (internal and/or C-terminal) recognized by rho-1D4 antibody used for immunoaffinity purification. Spectra measured in the dark (green line) and after illumination for 15 s with orange light (purple line) are shown. (*A*) Rhodopsin. (*B*) R–mVenus. (*C*) R–mVenusΔ. (*D*) Copurified rhodopsin and R–mVenus (1:1 molar ratio of plasmids used for transfection). (*E*) Copurified rhodopsin and R–mVenusΔ (1:2 molar ratio of plasmids used for transfection). The small contribution of mVenus to the absorption at ≈516 nm is attributable to the weak affinity of the rho-1D4 antibody for the internal epitope (see *C*). The results show that fluorescent-protein-tagged rhodopsin lacking the C-terminal epitope tag does not copurify with coexpressed wild-type rhodopsin. Analogously, coexpression of R–mVenus and wild-type rhodopsin lacking the 1D4 epitope yielded spectra very similar to R–mVenus alone (data not shown).

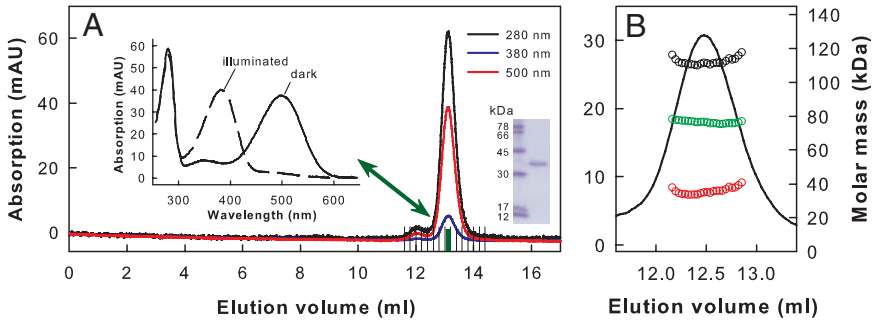

Fig. 3. SEC of rhodopsin purified from bovine disk membranes. (*A*) Typical chromatogram of rhodopsin purified in DDM detergent. The peak fraction highlighted in green was used for subsequent G_t activation experiments. *Inset* shows UV/visible absorption spectra of the highlighted fraction measured in the dark and after illumination for 15 s with orange light. This rhodopsin fraction typically had an A_{280}/A_{500} ratio below 1.6, indicating a purity close to 100%. (*Inset*) SDS gel of purified rhodopsin (right lane). (*B*) Online molar mass determination of purified dark-state rhodopsin in 0.03% (wt/vol) DDM by SEC in combination with MALLS detection. The calculated molar masses are shown as a function of elution volume for the rhodopsin–detergent complex (black circles). The calculated molar masses of protein and detergent in the rhodopsin–detergent complex are shown as red and green circles, respectively. The values obtained (35 kDa and 74 kDa) are close to the molar masses of rhodopsin (39 kDa; determined from the primary structure) and DDM micelles [74 kDa (49)].

maximum of R*; Fig. 4*C*). Analogously, the area of the GDP elution peak detected at 253 nm (absorption maximum of GDP) reflects the amount of GDP released upon R*·G_t complex formation. Normalization of the peak areas by the different extinction coefficients of R* and GDP yielded approximately the same values, i.e., equimolar amounts of R* and GDP (see figure legend and *Materials and Methods* for details). Accordingly, one GDP molecule was released from G_t·GDP upon interaction with R*, again consistent with a 1:1 R*·G_t complex.

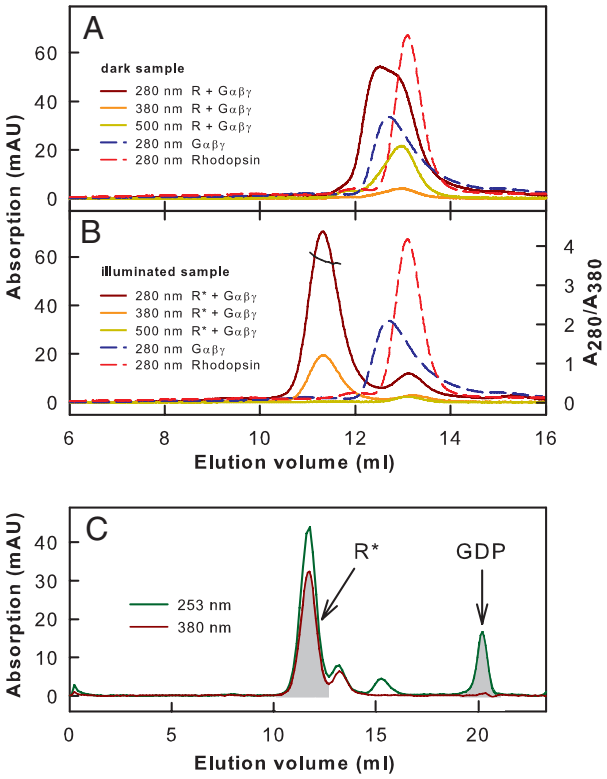

Fig. 4. Transducin binding to monomeric rhodopsin. (*A*) Superposition of SEC elution profiles: G_t holoprotein (Gαβγ) or rhodopsin (R; inactive ground state) alone (dashed lines) or as mixture (solid lines). (*B*) SEC elution profiles as in *A* obtained with R*. Detection occurred at the absorption maxima of protein (280 nm), R* (380 nm), and rhodopsin (500 nm). R*·G_t complex formation is indicated by a shift of the main elution peak. For this peak, a value of 3.6–3.8 was determined for the absorption ratio A_{280}/A_{380} (black line), which is consistent with a 1:1 stoichiometry between R* and G_t in the R*·G_t complex (theoretical values are 3.56 for R*:G_t = 1:1 and 2.52 for R*:G_t = 2:1; see *Materials and Methods*). (*C*) SEC elution profile of R*/G_t mixture detected at 380 nm (absorption maximum of R*) and 253 nm (absorption maximum of GDP). The ratio between peak areas corresponding to R* and GDP, respectively, ranges from 3.0 to 3.2 for different runs (theoretical values are 3.07 for R*:G_t = 1:1 and 6.13 for R*:G_t = 2:1; see *Materials and Methods*).

Analysis of G_t Activation by Monomeric Rhodopsin. For G_t activation measurements, we used the central fraction of the SEC elution peak, shown above to contain pure monomeric rhodopsin (Fig. 3*A*). To quantify the catalytic capacity of monomeric rhodopsin, we determined the initial rate of G_t activation by monitoring the intrinsic tryptophan fluorescence change of the G protein α-subunit, linked to GTPγS uptake (Fig. 5*A*). We first measured the activation rate [expressed as activated G_t molecules (G_t*) per second] as a function of rhodopsin concentration (R* = 0–3.0 nM; Fig. 5*A Inset*). The found linear dependence allowed the measured activation rates to be normalized to R*. To obtain the maximum velocity (V_{max}) of the reaction, we titrated the fluorescence changes with G protein up to a concentration of 12 μM G_t. The highest activation rate measured was ≈40 G_t*/R*·s (Fig. 5*B*). This is a lower limit because at higher G_t concentrations the rate decreased. Titration curves significantly deviate from the simple Michaelis–Menten type of hyperbolic curve, because of subunit dissociation at low G_t concentration and inhibition of R*/G_t interaction by the detergent (Fig. 5*B*). G_t interacts with detergent micelles because of its hydrophobic modifications, i.e., myristoylation of the α-subunit and farnesylation of the γ-subunit (25). Consistently, highest activation rates were obtained close to the critical micelle concentration of DDM [≈0.005% (wt/vol); Fig. 5*B Inset*]. In agreement with this finding, recombinant nonmyristoylated $G\alpha_{i1}/G_t\beta\gamma$ showed little detergent sensitivity (data not shown). At 0.006% (wt/vol) DDM, hyperbolic saturation was approached. Under these conditions, a Michaelis constant (K_m) of 0.55 μM was obtained when accounting for the detergent effect and G_t subunit dissociation [see *Materials and Methods* and supporting information (SI) *Methods* for details]. A maximal velocity (V_{max}) of 46 G_t*/R*·s was obtained by global fit to all data points (Fig. 5*B*). The enzymatic efficiency can be expressed as the ratio of the catalytic rate (k_{cat}) and K_m. The value obtained from our data is $k_{cat}/K_m = V_{max}/(R^*{\cdot}K_m) = 8.4{\cdot}10^7$ $M^{-1}{\cdot}s^{-1}$, which is close to the diffusion limit expected for the encounter of two proteins in solution (26) and shows that the catalytic interaction between monomeric rhodopsin and its G protein is very efficient.

Discussion

Our results show that in DDM detergent solution rhodopsin interacts with its cognate G protein G_t in a 1:1 stoichiometry and

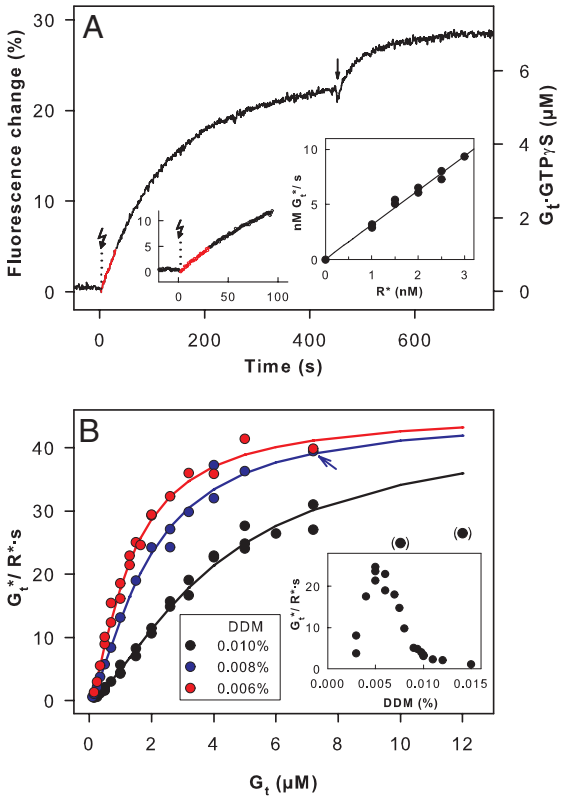

Fig. 5. G protein activation by monomeric rhodopsin. (*A*) Activation of G_t measured as tryptophan fluorescence increase attributable to GTPγS uptake [shown for 7.2 μM G_t, 1 nM R*, 200 μM GTPγS, and 0.008% (wt/vol) DDM at 20°C and pH 7.1]. Reactions were triggered by light activation (flash symbol) of rhodopsin. The arrow marks the point when additional R* was added to activate the whole G_t pool. (*Left Inset*) Same signal on expanded scale. Data points plotted in red were used for linear regression to determine reaction rate from initial slope of the fluorescence trace. See SI Fig. 6 for control experiments. (*Right Inset*) Reaction rates [nM activated G_t (G_t*) per second] as function of R* concentration [1 μM G_t, 0–3.0 nM R*, 0.01% (wt/vol) DDM]. (*B*) G_t activation rates plotted as a function of total G_t concentration [DDM concentration (wt/vol) as indicated]. Blue arrow indicates the data point (blue dot behind red dot) from the trace in *A*. Solid lines are best least-square fits of the data to a Michaelis–Menten type hyperbolic function, taking G_t subunit dissociation and G_t binding to detergent micelles into account. The numerical global fit yielded for all curves V_{max} = 46 G_t*/R*·s, K_1 = 0.46 μM (G_t subunit dissociation), and K_2 = 1.76 μM (G_t micelle binding). K_m values are 0.55 μM (0.006% DDM), 0.8 μM (0.008% DDM), and 2.3 μM (0.01% DDM). For recombinant rhodopsin and G_t, a similar rate profile was obtained [0.01% (wt/vol) DDM; data not shown]. (*Inset*) G_t activation rates (1 μM G_t) as a function of DDM detergent concentration.

that the rhodopsin monomer also is competent to activate G_t with a rate close to the physical limit in solution. The maximum rate in the native membrane still is about one order of magnitude higher than in solution (27, 28). This finding may be explained by the reduction in translational degrees of freedom in a two-dimensional membrane, which facilitates successful coupling. Fast and immediate docking is enabled by the precise orientation of the G protein to the membrane surface. The membrane anchor of the G protein made up of the myristoyl/farnesyl modifications at the α- and γ-subunits, respectively (25, 29, 30), now can play a decisive role in the initial encounter between the proteins. Evidence for a sequential interaction between different binding sites on G_t and R*, which includes such a docking process, recently was presented (30, 31). Computational modeling suggested a single rhodopsin molecule to be sufficient for docking of G_t (32, 33). It remains to be elucidated whether a pairing of rhodopsin in disk membranes further improves the overall speed of catalytic G_t activation.

Materials and Methods

Materials. All materials and purified anti-rhodopsin monoclonal antibody rho-1D4 were as described in ref. 34. Buffer A was 20 mM 1,3-bis[Tris(hydroxymethyl)methylamino]propane (pH 7.1), 130 mM NaCl, and 1 mM $MgCl_2$.

Construction of R–mVenus, R–mECFP, and mVenus–mECFP Fusion Plasmids. The mammalian cell expression vector pMT4 containing a synthetic opsin gene was modified by standard cloning and PCR procedures such that the opsin gene was followed by bases GGATCAACCGGT (the AgeI site is underlined), then followed by the gene corresponding to the monomeric fluorescent proteins mECFP or mVenus and codons corresponding to the amino acid sequence GTETSQVAPA. Rhodopsin's C-terminal sequence ETSQVAPA is recognized by the rho-1D4 antibody used for immunoaffinity purification of the fusion proteins (35). The fluorescent proteins used were variants of GFP. The cyan variant mECFP is *Aequorea victoria* GFP with mammalian codons and the following additional mutations: K26R, F64L, S65T, Y66W, N146I, M153T, V163A, N164H, H231L, a Val-1a insertion (see Clontech Laboratories, Mountain View, CA, and ref. 36), and A206K. The A206K mutation introduced with the QuikChange kit (Stratagene, La Jolla, CA) causes parental ECFP (weakly dimeric) to monomerize (37). The yellow variant mVenus is *Aequorea victoria* GFP with mammalian codons and the following additional mutations: F46L, F64L, S65G, V68L, S72A, M153T, V163A, S175G, T203Y, H231L, a Val-1a insertion (38), and A206K [to avoid dimerization (37)]. The control construct mVenus–mECFP was cloned by replacing the EcoRI–SalI fragment of R–mECFP with the mVenus gene. The gene product corresponds to a fusion protein of mVenus and mECFP separated by a 20-aa linker sequence. In the plasmid R–mVenusΔ, bases corresponding to the C-terminal amino acid sequence GTETSQVAPA were deleted. All constructs were verified by DNA sequencing.

Expression and Purification of Rhodopsins. Rhodopsin, R–mVenus, R–mECFP, and mVenus–mECFP fusion proteins were expressed in COS-1 cells by using a diethylamino-ethyl (DEAE)-dextran transfection procedure. The cells were harvested 72 h after transfection, and 11-*cis*-retinal was added to reconstitute rhodopsin (34, 39). The expressed proteins were purified by using a rho-1D4–Sepharose immunoaffinity matrix as described (34, 39). All procedures were carried out under dim red light. Briefly, cells were harvested in PBS buffer (137 mM NaCl, 2.7 mM KCl, 8.1 mM Na_2HPO_4, and 1.5 mM KH_2PO_4, pH 7.4) and reconstituted with 11-*cis*-retinal (30 μM final concentration) for 12 h at 6°C. Cells were solubilized in 1% (wt/vol) DDM for 2–4 h at 6°C and then incubated with rho-1D4–Sepharose matrix overnight. For protein purification, the matrix was washed repetitively in a batch procedure using centrifugation to separate matrix and solution. Wash steps were performed twice with 0.03% (wt/vol) DDM in PBS and then once or twice with 0.03% (wt/vol) DDM in 10 mM 1,3-bis[Tris(hydroxymethyl)methylamino]propane (BTP), pH 6.0. Immunoaffinity-purified protein was eluted from the matrix by adding 150 μM peptide corresponding to the C-terminal 18 aa of rhodopsin (3–4 h, 6°C). The eluted protein was separated from the matrix by centrifugation.

Preparation of Transducin. G_t was prepared from bovine rod outer segments and in most cases was separated into Gα and Gβγ subunits by chromatography as described in ref. 27. G_t or its separated subunits (8–15 ml) were incubated with 0.5-ml Con A Sepharose 4B beads (GE Healthcare, Barrington, IL) at 6°C for 1 h to remove traces of rhodopsin. G_t or separated G_t subunits

then were dialyzed against buffer A containing 2 mM DTT. Dialyzed G_t or G_t subunits were concentrated by ultrafiltration using Centricon YM-10 concentrators (Millipore, Billerica, MA) and stored on ice until use. Protein concentration was determined with Bradford reagent. The final G_t concentration ranged between 30 and 40 μM. To determine the amount of activatable G_t, G_t was titrated with exact amounts of GTPγS (250 nM) in the presence of 500 nM R* under constant stirring in a final volume of 700 μl (40). GTPγS concentration was determined by UV/visible absorption spectroscopy with $\varepsilon_{253} = 13{,}700\ M^{-1}\cdot cm^{-1}$ (41). All calculated activation rates in this work refer to the amount of activatable G_t as determined by GTPγS titration.

Preparation of Bovine Rhodopsin and SEC. Rod outer segment membranes were prepared as described in ref. 27. After incubation of the rod outer segment membranes (150 μM rhodopsin) with 5 μM 11-*cis*-retinal for 30 min at 4°C, DDM was added to a final concentration of 1.4% (wt/vol) followed by further incubation for 3 h. Unsolubilized material was removed by ultracentrifugation. Solubilized rhodopsin was purified by using the 1D4-immunoaffinity procedure described above (four wash steps). Then, 100 μl of purified rhodopsin was applied at a flow rate of 300 μl/min and 14–18°C to a Tricorn Superdex 200 300/10 GL column (GE Healthcare) equilibrated with buffer A containing 1 mM DTT and 0.03% (wt/vol) DDM by using a SMART system and SMART Manager software (Amersham Pharmacia/GE Healthcare). The same setup and buffer A containing 0.03% (wt/vol) DDM (with or without 1 mM DTT) was used for SEC of purified rhodopsin with G_t at different temperatures (4–12°C). Light activation of rhodopsin was performed as described below.

UV/Visible Spectroscopy. Absorption spectra were taken at 20°C with a Cary 50 Bio UV/visible spectrophotometer (Varian, Palo Alto, CA) with a resolution of 1 or 2 nm. For each sample, absorption spectra between 250 and 650 nm were recorded in the dark and after illumination of the sample for 15 s with orange light with a 150-W fiber-optic light source equipped with a long-pass filter (GG 495; Schott, Elmsford, NY) and a heat-protection filter.

Molar Extinction Coefficients for Analysis of UV/Visible Absorption Data. The following molar extinction coefficients were assumed: rhodopsin $\varepsilon_{500} = 40{,}600\ M^{-1}\cdot cm^{-1}$ (42), rhodopsin $\varepsilon_{280} = 65{,}000\ M^{-1}\cdot cm^{-1}$ (with an $A_{280\ nm}/A_{500\ nm}$ ratio of $\approx$1.6), R* (metarhodopsin II) $\varepsilon_{380} = 42{,}000\ M^{-1}\cdot cm^{-1}$ (43), $\varepsilon_{280} = 61{,}800\ M^{-1}\cdot cm^{-1}$ [in metarhodopsin II, ε_{280} is $\approx$5% lower compared with rhodopsin (44)], G_t α-subunit $\varepsilon_{280} = 30{,}400\ M^{-1}\cdot cm^{-1}$, G_t $\beta\gamma$-subunit $\varepsilon_{280} = 57{,}400\ M^{-1}\cdot cm^{-1}$, and G_t ($\alpha\beta\gamma$) $\varepsilon_{280} = 87{,}800\ M^{-1}\cdot cm^{-1}$. The values for G_t were calculated with Swiss-Prot entries GNAT1_BOVIN, GBB1_BOVIN, and GBG1_BOVIN with the ExPASy (www.expasy.org) ProtParam tool (45). The tool used the Edelhoch method (46) and extinction coefficients for Trp and Tyr determined by Pace *et al*. (47).

Calculation of the A_{280}/A_{380} Ratio of the R*·G_t Complex. For determination of the stoichiometry of R* and G_t in the R*·G_t complex from UV/visible absorption data obtained by SEC, the ratio of the absorption of the protein moiety in the R*·G_t complex to the retinal chromophore absorption was calculated as follows:

$$A_{280\ nm}/A_{380\ nm} = (61{,}800 + 87{,}800)/42{,}000$$
$$= 3.56 \text{ for a 1:1 (R*:}G_t\text{) stoichiometry}$$

and

$$A_{280\ nm}/A_{380\ nm} = (2\cdot 61{,}800 + 87{,}800)/2\cdot 42{,}000$$
$$= 2.52 \text{ for a 2:1(R*:}G_t\text{) stoichiometry.}$$

Calculation of GDP Released per R*·G_t Complex. SEC runs with R*/Gt mixtures were performed with detection at 253 nm to monitor GDP ($\varepsilon_{253} = 13{,}700\ M^{-1}\cdot cm^{-1}$; ref. 41) and 380 nm to monitor R* ($\varepsilon_{380} = 42{,}000\ M^{-1}\cdot cm^{-1}$, see above). Release of one molecule of GDP per R*·G_t complex is given by the ratio of peak areas:

$$\text{Area(R*, 380 nm)/Area(GDP, 253 nm)}$$
$$= 42{,}000/13{,}700$$
$$= 3.07 \text{ for a 1:1 (R*:}G_t\text{) stoichiometry}$$

and

$$\text{Area(R*, 380 nm)/Area(GDP, 253 nm)}$$
$$= 2\cdot 42{,}000/13{,}700$$
$$= 6.13 \text{ for a 2:1 (R*:}G_t\text{) stoichiometry.}$$

MALLS. For mass determination, a combined setup consisting of SEC and subsequent online detection by UV absorption, three-angle static MALLS and differential refractive index measurement was used (48). SEC was performed with a Tricorn Superdex 200 10/300 GL column (GE Healthcare) connected to an ÄKTA purifier chromatography system (GE Healthcare) equilibrated with buffer A containing 1 mM DTT and 0.005 or 0.03% (wt/vol) DDM, respectively. For MALLS and differential refractive index measurements, a linear coupled miniDAWN Tristar system (Wyatt Technology, Santa Barbara, CA) and a differential refractive index detector (RI-101; Shodex, Kawasaki, Japan), respectively, were used. All calculations were performed with the software ASTRA (Wyatt Technology) on the basis of the detected signals for the UV absorption (280 nm), the refractive index (49), and three different scattering angles of scattered laser light. Experiments were performed at 4–6°C. Each experiment was repeated at least in triplicate. Under both detergent conditions of SEC, 0.005% or 0.03% (wt/vol) DDM, rhodopsin eluting in the SEC peak fraction was monomeric. For calculation of the molar masses, an extinction coefficient (at 280 nm) of $1{,}667\ ml\cdot g^{-1}\cdot cm^{-1}$ for rhodopsin and a dn/dc value of 0.133 for DDM (49) was used. Effects of interdetector band broadening between instruments in the online experiment were corrected by using ASTRA software.

Transducin Activation Assay. As a monitor for G_t activation, changes in intrinsic fluorescence intensity of the Gα-subunit upon exchange of GDP to GTPγS were quantified (40). All measurements were carried out by using a SPEX fluorolog II spectrofluorometer equipped with a 450-W xenon arc lamp. For all activation measurements, settings were $\lambda_{ex} = 300$ nm and $\lambda_{em} = 345$ nm with an integration time of 1 s. G_t activation rates were measured with 0–3 nM purified rhodopsin, 200 μM GTPγS, buffer A, 2 mM DTT, and 0.003–0.015% (wt/vol) DDM in a final volume of 80 μl (3 × 3 mm cuvette) or 650 μl (10 × 4 mm cuvette with stirring bar). All samples were equilibrated at 20°C for 4 min. Reactions were triggered with orange light (Schott GG 495 long-pass filter) after recording basic fluorescence levels for 50 s. After recording the activation at the respective R* concentration, activation of the whole G_t pool was achieved by adding 5 nM purified rhodopsin to the reaction. The maximal amplitude of fluorescence after addition of excess rhodopsin accounts for the total amount of G_t in the sample. Thus, the change in fluorescence (F/t) translates into activated

G_t molecules per second. The whole set of experiments was repeated with different G_t and rhodopsin preparations.

The initial G_t activation rate (v) was obtained by linear regression of the initial rise in fluorescence emission. The fluorescence change was titrated with G_t, and the data points were fitted to a Michaelis–Menten type hyperbolic function: $v = (V_{max}\cdot[G\alpha\beta\gamma])/(K_m + [G\alpha\beta\gamma])$,

where V_{max} and K_m denote the maximum value of v and the Michaelis constant, respectively, and $[G\alpha\beta\gamma]$ is the effective G_t concentration. $[G\alpha\beta\gamma]$ was calculated numerically in the fitting procedure by assuming that a fraction of the added G_t dissociates into its $G\alpha$ and $G\beta\gamma$ subunits (with a dissociation constant K_1) or binds to detergent micelles without rhodopsin (with a dissociation constant K_2; see *SI Methods*). The data points of the titration experiments performed at three different DDM concentrations (0.01%, 0.008%, and 0.006%) were simultaneously fitted with the same set of parameters V_{max}, K_1, and K_2 but with individual Michaelis constants (K_{m1}, K_{m2}, and K_{m3}). DDM micelle concentration was set to 1.2 μM (0.006% DDM), 1.6 μM (0.008% DDM), and 2 μM (0.01% DDM).

FRET Experiments. Fluorescence emission spectra between 450–600 nm (excitation at 420 nm) and 520–600 nm (excitation at 510 nm) of fluorescent proteins were recorded at 20°C with a SPEX fluorolog II spectrofluorometer and corrected for the fluorescence emission of the buffer. To determine FRET between mECFP and mVenus, the spectra of 11-*cis*-retinal-reconstituted purified R–mECFP and copurified R–mECFP/R–mVenus, respectively, were compared. Direct excitation of R–mVenus by the 420-nm excitation beam in the R–mECFP/R–mVenus mixture was accounted for as follows. (*i*) The emission spectrum of the R–mVenus reference sample (excitation at 420 nm) was scaled to the amount present in the R–mECFP/R–mVenus mixture by comparing maximal mVenus emission at 530 nm (excitation at 510 nm). (*ii*) The scaled R–mVenus emission spectrum (excitation at 420 nm) then was subtracted from the emission spectrum of the R–mECFP/R–mVenus mixture (excitation at 420 nm). The difference spectrum of the corrected R–mECFP/R–mVenus spectrum and the R–mECFP spectrum (matched to the peak height at 480 nm) yields the emission attributable to FRET. The same procedure was applied to analyze the mVenus–mECFP fusion protein. For the measurement, purified samples were diluted with 2 vol of buffer A containing 2 mM DTT, yielding a final concentration of 0.01% (wt/vol) DDM and 0.75 μM protein.

We thank Ingrid Semjonow for technical assistance and Arturo Zychlinsky and Cordula Enenkel for critically reading the manuscript. This work was supported by Deutsche Forschungsgemeinschaft Grants Sfb449 and Sfb740.

1. Foord SM, Bonner TI, Neubig RR, Rosser EM, Pin JP, Davenport AP, Spedding M, Harmar AJ (2005) *Pharmacol Rev* 57:279–288.
2. Neves SR, Ram PT, Iyengar R (2002) *Science* 296:1636–1639.
3. Liebman PA, Parker KR, Dratz EA (1987) *Annu Rev Physiol* 49:765–791.
4. Fotiadis D, Liang Y, Filipek S, Saperstein DA, Engel A, Palczewski K (2003) *Nature* 421:127–128.
5. Salom D, Lodowski DT, Stenkamp RE, Le Trong I, Golczak M, Jastrzebska B, Harris T, Ballesteros JA, Palczewski K (2006) *Proc Natl Acad Sci USA* 103:16123–16128.
6. George SR, O'Dowd BF, Lee SP (2002) *Nat Rev Drug Discov* 1:808–820.
7. Terrillon S, Bouvier M (2004) *EMBO Rep* 5:30–34.
8. Milligan G (2004) *Mol Pharmacol* 66:1–7.
9. Meyer BH, Segura JM, Martinez KL, Hovius R, George N, Johnsson K, Vogel H (2006) *Proc Natl Acad Sci USA* 103:2138–2143.
10. James JR, Oliveira MI, Carmo AM, Iaboni A, Davis SJ (2006) *Nat Methods* 3:1001–1006.
11. Filipek S, Krzysko KA, Fotiadis D, Liang Y, Saperstein DA, Engel A, Palczewski K (2004) *Photochem Photobiol Sci* 3:628–638.
12. Filizola M, Wang SX, Weinstein H (2006) *J Comput Aided Mol Des* 20:405–416.
13. Ciarkowski J, Witt M, Slusarz R (2005) *J Mol Model* 11:407–415.
14. Mansoor SE, Palczewski K, Farrens DL (2006) *Proc Natl Acad Sci USA* 103:3060–3065.
15. Kota P, Reeves PJ, Rajbhandary UL, Khorana HG (2006) *Proc Natl Acad Sci USA* 103:3054–3059.
16. Botelho AV, Huber T, Sakmar TP, Brown MF (2006) *Biophys J* 91:4464–4477.
17. Jastrzebska B, Maeda T, Zhu L, Fotiadis D, Filipek S, Engel A, Stenkamp RE, Palczewski K (2004) *J Biol Chem* 279:54663–54675.
18. Jastrzebska B, Fotiadis D, Jang GF, Stenkamp RE, Engel A, Palczewski K (2006) *J Biol Chem* 281:11917–11922.
19. Filipek S, Stenkamp RE, Teller DC, Palczewski K (2003) *Annu Rev Physiol* 65:851–879.
20. Fotiadis D, Jastrzebska B, Philippsen A, Muller DJ, Palczewski K, Engel A (2006) *Curr Opin Struct Biol* 16:252–259.
21. Palczewski K (2006) *Annu Rev Biochem* 75:743–767.
22. Chabre M, Cone R, Saibil H (2003) *Nature* 426:30–31.
23. Chabre M, le Maire M (2005) *Biochemistry* 44:9395–9403.
24. Hofmann KP, Spahn CM, Heinrich R, Heinemann U (2006) *Trends Biochem Sci* 31:497–508.
25. Bigay J, Faurobert E, Franco M, Chabre M (1994) *Biochemistry* 33:14081–14090.
26. Berg OG, von Hippel PH (1985) *Annu Rev Biophys Biophys Chem* 14:131–160.
27. Heck M, Hofmann KP (2001) *J Biol Chem* 276:10000–10009.
28. Burns ME, Arshavsky VY (2005) *Neuron* 48:387–401.
29. Seitz HR, Heck M, Hofmann KP, Alt T, Pellaud J, Seelig A (1999) *Biochemistry* 38:7950–7960.
30. Herrmann R, Heck M, Henklein P, Henklein P, Kleuss C, Hofmann KP, Ernst OP (2004) *J Biol Chem* 279:24283–24290.
31. Herrmann R, Heck M, Henklein P, Hofmann KP, Ernst OP (2006) *J Biol Chem* 281:30234–30241.
32. Fanelli F, Dell'Orco D (2005) *Biochemistry* 44:14695–14700.
33. Dell'Orco D, Seeber M, Fanelli F (2007) *FEBS Lett* 581:944–948.
34. Fritze O, Filipek S, Kuksa V, Palczewski K, Hofmann KP, Ernst OP (2003) *Proc Natl Acad Sci USA* 100:2290–2295.
35. Molday RS, MacKenzie D (1983) *Biochemistry* 22:653–660.
36. Griffin BA, Adams SR, Tsien RY (1998) *Science* 281:269–272.
37. Shaner NC, Steinbach PA, Tsien RY (2005) *Nat Methods* 2:905–909.
38. Nagai T, Ibata K, Park ES, Kubota M, Mikoshiba K, Miyawaki A (2002) *Nat Biotechnol* 20:87–90.
39. Meyer CK, Böhme M, Ockenfels A, Gärtner W, Hofmann KP, Ernst OP (2000) *J Biol Chem* 275:19713–19718.
40. Ernst OP, Bieri C, Vogel H, Hofmann KP (2000) *Methods Enzymol* 315:471–489.
41. Bock RM, Ling NS, Morell SA, Lipton SH (1956) *Arch Biochem Biophys* 62:253–264.
42. Wald G, Brown PK (1953) *J Gen Physiol* 37:189–200.
43. Matthews RG, Hubbard R, Brown PK, Wald G (1963) *J Gen Physiol* 47:215–240.
44. Lin SW, Sakmar TP (1996) *Biochemistry* 35:11149–11159.
45. Gasteiger E, Hoogland C, Gattiker A, Duvaud S, Wilkins MR, Appel RD, Bairoch A (2005) in *The Proteomics Protocols Handbook*, ed Walker JM (Humana, Totowa, NJ), pp 571–607.
46. Edelhoch H (1967) *Biochemistry* 6:1948–1954.
47. Pace CN, Vajdos F, Fee L, Grimsley G, Gray T (1995) *Protein Sci* 4:2411–2423.
48. Wen J, Arakawa T, Philo JS (1996) *Anal Biochem* 240:155–166.
49. Strop P, Brunger AT (2005) *Protein Sci* 14:2207–2211.